

BENDING MAGNETS FOR THE CBA BEAM TRANSPORT LINE\*

R.E. Thern  
Brookhaven National Laboratory, Upton, New York 11973

Summary

The beam transport line from the AGS to CBA requires 68 large bending magnets, consisting of pure dipoles and two types of combined function gradient magnets. All three types were designed with the magnetic field calculation program POISSON, using the same exterior dimensions and coil package. The design goal of  $\pm 1\%$  momentum acceptance for the transport line required a wide horizontal aperture, with a much smaller vertical aperture for economy. Two prototypes of one gradient magnet were built, and a facility constructed to measure them and the later production magnets. Measurements were done using both a long coil and a point coil (Rawson-Lush gaussmeter). Preliminary results show  $\Delta B/B < 0.2 \times 10^{-3}$ ,  $\Delta G/G < 0.3 \times 10^{-2}$ , and  $\Delta B_2/B < 0.3 \times 10^{-4} \text{ cm}^{-2}$  over the beam aperture. Due to end effects, the actual gradient differs from the design gradient by 1%, which has been compensated for in the beam line design.

Magnet Parameters

The parameters for the three types of bending magnets are shown in Table I; further information is in reference 1. Type C is used for the  $20^\circ$  bend of the existing AGS fast-extracted beam line, type B is for the two opposite  $90^\circ$  bends into the two rings of CBA, and type A is for the matching sections before CBA injection. Type C is 3.6576 m long; the others are used in both 3.6576 and 2.9464 m lengths.

Table I. Transport Line Magnet Parameters

Type	B(kG)	G(kG/cm)	gap(mm)	Amp-Turn
A	15.82	0	29	36508
B	12.55	0.369	32	32366
C	11.70	0.231	39	36311

Design

All three types of magnet were designed using the magnetic field calculation program POISSON.<sup>2</sup> The exact hyperbolic contour for a gradient magnet was modified by trial-and-error to reduce the effects of saturation and to attain the required good field width with a minimum overall magnet size. On the high field side of the gradient magnet (and on both sides of the dipole) saturation of the iron greatly reduces the good field width if not corrected. Several configurations of tapering the side of the pole were tried, and one chosen which maximized the extent of the good field at high excitation, and which also had small differences between high and low excitation field shapes. Then the good field region was extended further on both sides with small shims, whose size was close to that determined analytically,<sup>3</sup> but was actually determined empirically. Finally, small corrections were made to the central, curved part of the magnet profile to optimize the field shape at full design excitation. At lower fields as might be used for example for lower momentum injection into CBA, the calculated field is still satisfactory.

All three magnet types require approximately the same width for the pole root, and have comparable total flux in the return yoke. Thus for economy of

construction, all are designed so they differ only in the pole face, allowing the same stacking fixture and other production hardware to be used for all. Figure 1 shows the cross section of the type B magnet.

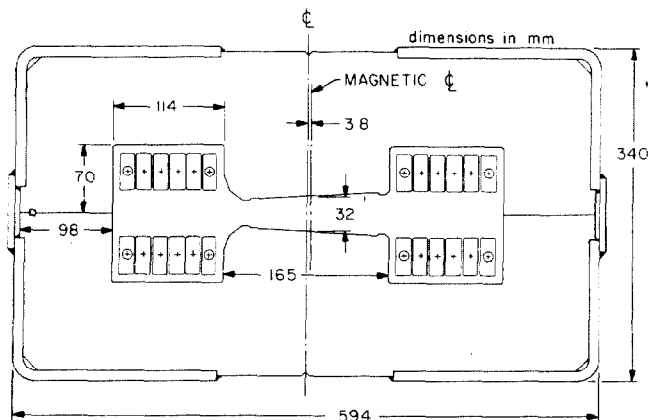


Figure 1. Cross section of Type B magnet.

The three also require nearly the same ampere-turns, so all use the same coil. The coil is a flat single-layer pancake in which the turns are insulated by epoxy-fiberglass spacers and epoxy potting. It is built with four terminals, in a  $5\frac{1}{2} + 1\frac{1}{2}$  turn configuration. This will allow the magnets to be interconnected from both ends, with no bus work running the length of the magnet.

Measurement

Two prototype magnets of type B, used in the  $90^\circ$  bends, have been constructed for initial testing. The results given here are from one of these magnets. Initial magnets of other types from a partial production order are just now being completed and will be tested soon.

A facility has been constructed for measuring these magnets to the required accuracy. A tolerance analysis of the transport line<sup>1</sup> showed that the fields must be correct to  $1 \times 10^{-3}$ ; therefore to be safe a goal of  $1 \times 10^{-4}$  was set for each variable to be measured.

Because of the small aperture of the magnet, it was not possible to insert a full-length coil on a coil form and provide the necessary support inside the magnet. A full-length coil of the required small diameter would be quite flexible, and in the stronger of the gradient magnets would require positioning over its entire length to within  $10^{-4} \text{ B/G} = 0.03 \text{ mm}$  to get a measurement meaningful to  $1 \times 10^{-4}$  of the field. Since there are no supports available other than the curved face of the pole, this was not considered practical. Instead, two other methods were implemented - a small "point" coil on a long probe, supported and positioned from outside the magnet, and a long coil of stretched wires without a coil form.

Long Wire Measurement

The long wire scheme measures the integrated B dl of the magnet as a function of transverse position. The coil consists of six turns of 5-mil tungsten wire

\* Work performed under the auspices of the U.S. Department of Energy.

with a cross section approximately 6 mm square. The wires are wound around separate pulleys at each end, and are stretched to about half their breaking strength to minimize sag. The two ends are rotated and translated independently. For insertion into or removal from a magnet, the two ends of the coil can be fastened to a strongback which is small enough to be fitted through the magnet aperture, and thus the coil can be transported from one magnet to another without the wires losing tension and falling off their pulleys.

As the apparatus is rotated at about 0.5 Hz, the induced voltage is sampled at 1 msec intervals with a 16-bit ADC. The large amount of noise from the free vibrations of the wire at about 26 Hz is reduced with a low-pass filter, and is further reduced by doing a Fourier analysis for the 0.5 Hz signal. Initial results from this method look promising, and it is intended to develop it as a system for production testing.

### Point Coil Measurement

The results presented here were obtained by making precision "point" measurements as a function of position, using a Rawson-Lush Model 920 gaussmeter,<sup>4</sup> positioned using the lengthwise travel and cross feed of a large lathe. Figures 2 and 3 show a block diagram and a schematic representation of the apparatus. The Model 920 gaussmeter derives its signal from a small coil, about 3 mm in diameter, rotating at 30 Hz at the end of a 125 cm shaft. On the same shaft, outside the magnetic field, is a reference generator in a temperature controlled oven. The signal from the reference generator is divided by a precision decade ratio transformer and used to null out the unknown signal. The accuracy thus depends on the stability of the reference generator and the accuracy of the ratio transformer, and a level of 0.01% is advertised.

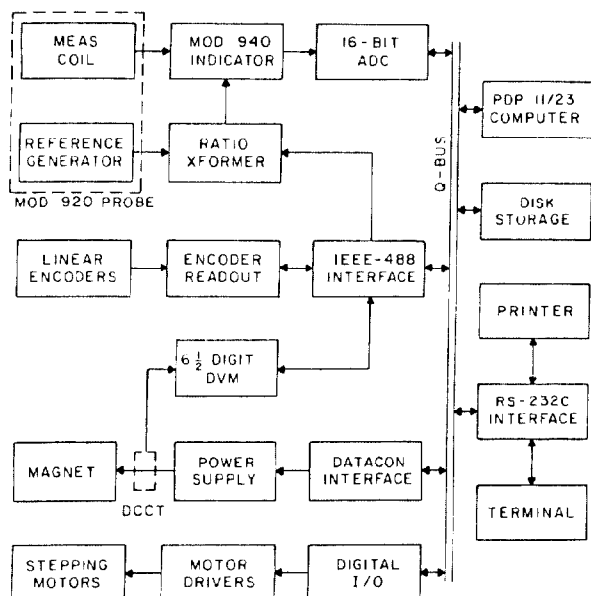


Figure 2. Block diagram of point coil measuring system.

The probe is moved using stepping motors to turn the lead screws of the lathe. The actual position is read using linear encoders of the type commonly used in machine shops; the least count of the encoders is 0.002 mm in the transverse (x) direction and 0.01 mm in the lengthwise (z) direction.

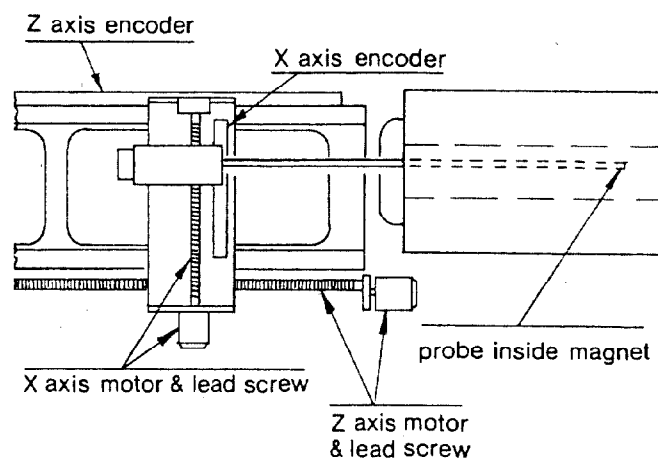


Figure 3. Top view of point measuring apparatus.

Because the coil in the gaussmeter is so far away from the position encoders, there is a large potential for error if the angle of the apparatus were to change slightly, as could happen when the direction of travel is reversed. Therefore, all measurements are made with the probe travelling in the same direction.

The probe is able to reach the entire usable width of the magnet on the midplane, up to a depth of about 80 cm from the end of the magnet. In operation, the field is mapped out on a rectangular grid in the z and x directions. Typical step sizes were 1.27 mm (0.05") in x, and 12.7 mm (0.5") in z, with finer steps in z, 3.175 mm (0.125"), in the region of change around the end of the magnet. About 6 to 10 seconds is required for each point, and a typical measurement involves several hours of unattended operation measuring several thousand points.

### Measurement Corrections and Errors

The measurements can suffer from errors in the gaussmeter reading, the position, and the magnet current. To estimate the statistical errors, the data at a fixed z are compared to a polynomial fit in x, of order high enough to show no systematic deviations; this shows a statistical error of about 0.5 Gauss rms in the measurements or  $\Delta B/B = 0.4 \times 10^{-4}$ . Several corrections have been applied to attain this value. First, the probe travel in z deviates from a straight line by about 0.25 mm due to imperfections in the lathe ways; this has been mapped and a correction applied. Second, all data combined show, by using the gradient of the magnet as a sensitive position monitor, a sine wave "ripple" in actual probe x position versus x encoder reading, of amplitude  $\pm 6 \times 10^{-3}$  mm and wavelength 5.08 mm, apparently due to turning of the x motion lead screw which has a pitch of  $0.2'' = 5.08$  mm. Finally, the power supply varied, at times, by as much as several Amperes (out of 2700). The data were all corrected to 2700 A, but the correction is imperfect due to hysteresis effects. In fact, this current variation is believed to be the major source of the statistical error; a recent measurement of an ACS main ring magnet using this equipment, but with the power supply better stabilized, shows noise less than 0.2 G rms.

It should be noted that measurements such as these depend critically on a proper conditioning of the magnet. When cycling the magnet up to 3150 A, the difference at 2700 A between the rising and falling parts of the hysteresis curve is 60 G, or  $5 \times 10^{-3}$  of the field.

### Longitudinal Field Distribution

Figure 4 shows the field along the magnetic centerline of the magnet. Apparent in the expanded scale are dips up to 0.4%; these are due to a distortion of the magnet core where the laminations are welded to the side angles, every 30 cm along the length of the magnet. Changes have been made in the design to reduce this effect for the production magnets; mechanical measurements in the first production unit - not yet tested magnetically - show the effect reduced but not eliminated.

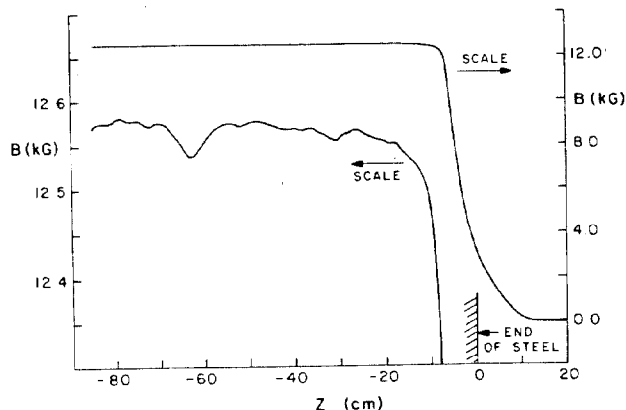


Figure 4. Longitudinal field distribution for Type B magnet,  $Z < 0$  is inside the magnet,  $Z > 0$  outside.

### Transverse Field Distribution

The reduction of the point measurements to an effective  $Bdz$  integral, as a function of  $x$ , is done in two steps. First, each sweep across the magnet at a fixed  $z$  is fitted by a polynomial function; twenty coefficients are used here, which allows the fit to follow the data over the entire measured width to well within the noise level. Then the fit coefficients, as a function of  $z$ , are integrated to get an effective fit for the integrated field. Since the entire length of the magnet is not measured, the fit for the accessible part of the interior is scaled appropriately and added to the fit for the end region to synthesize a result for an entire magnet.

The results are shown, for the field and its first two derivatives, in Figure 5. The field is graphed with the pure design gradient contribution subtracted to allow an expanded scale, any slope then shows a deviation from the design gradient. For the synthesized full magnet, the integrated  $Bdz$  has been divided by 3.6576 m. Also shown in the figure is the field calculated by POISSON. The calculated field is for the lamination as specified in the design; possible errors in the lamination as punched are not represented. The waviness of the second derivative plot is an artifact of the polynomial fit, but the general trend is real.

The figure shows the following about the performance of this magnet:

1. The field has a pure gradient form within  $\Delta B/B < 0.2 \times 10^{-3}$  over a 10 cm aperture.
2. The average gradient is 365 G/cm for the entire magnet, and 370 G/cm for the interior only. The end effects have decreased the gradient by 1.5% from the original design. This change has been compensated for in the beam line design. A proportional effect is also foreseen in the type C magnet, and the design gradient has been adjusted before production.

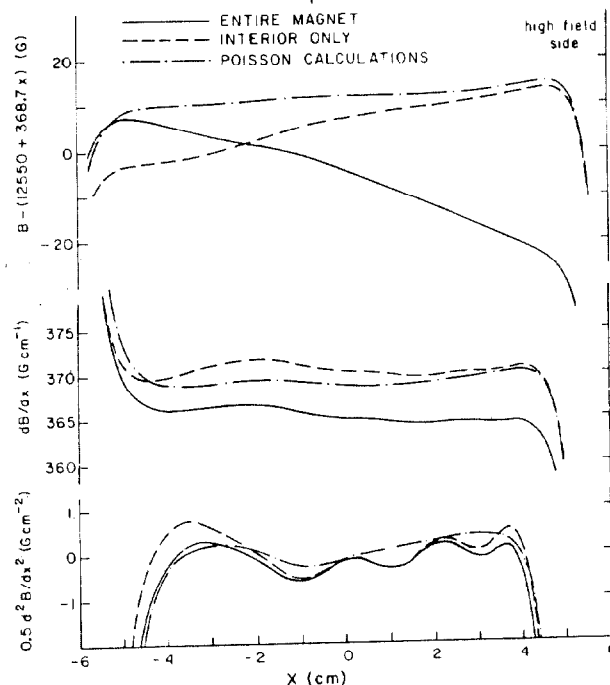


Figure 5. Transverse field distribution for Type B magnet.

3. The gradient is uniform with  $\Delta G/G < 0.3 \times 10^{-2}$  over a 9 cm width.
4. The local sextupole component has an average value  $b_2 = 0.17 \text{ G cm}^{-2}$ , but varies over the aperture by  $\pm 0.4 \text{ G cm}^{-2}$ . Thus  $b_2/B < 0.3 \times 10^{-4} \text{ cm}^{-2}$  except at the very edge of the aperture.

These results are within the limits specified in reference 1.

The point measurement field map will also allow a more detailed study of the optical properties of the magnet. J. Claus<sup>5</sup> has written a program which does ray tracing using the measured field values; this will be used to determine the exact Twiss parameters for a cell, and to find the optimum transverse offset between the focusing and defocusing elements of a cell to maximize the usable aperture.

### Acknowledgments

The author wishes to thank J.G. Keohane for the mechanical design of the magnet, A. Leskiewicz, P. Montemurro, and P. Zuhoski for the set up and operation of the measurement apparatus, and H. Foelsche for guidance on the entire transport line project.

### References

1. W.T. Weng, The Lattice Design and Tolerance Analysis of the CBA Transport Line, this conference.
2. R. Holsinger, POISSON, LAUR-76-2028.
3. J.J. Wilkins and A.H. Spurway, Rutherford Lab Report NIRL/R/6, 1961.
4. Rawson-Lush Instrument Co., Acton, MA.
5. J. Claus, BNL, private communication.